

# The complex molecular absorption line system at $z=0.886$ towards PKS1830–211

Tommy Wiklind

*Onsala Space Observatory, S-43992 Onsala, Sweden; (tommy@oso.chalmers.se)*

and

Françoise Combes

*DEMIRM, Observatoire de Paris, 61 Av. de l'Observatoire, F-75014 Paris, France; (bottaro@obspm.fr)*

## ABSTRACT

New single dish and millimeter wave interferometer observations of the molecular absorption line system in the gravitational lens to PKS1830–211 at  $z=0.88582$  is presented. Self-calibrated interferometer data shows unequivocally that the previously detected absorption component is associated with the gravitationally lensed south–west image of the background source. A second absorption line of  $\text{HCO}^+(2\leftarrow 1)$  at  $z=0.88582$  is detected. This component is shifted in velocity by  $-147 \text{ km s}^{-1}$  relative to the main absorption line, and is shown to be associated with the north–east image. A few additional absorption lines are presented. Upper limits to absorption and emission lines from the possible absorption system at  $z=0.1927$ , seen in 21 cm HI by Lovell et al, are reported. Alternatively, there could be only one absorbing system at  $z=0.88582$ , with the HI line attributed instead to the PS molecule.

*Subject headings:* ISM : molecules — BL Lacertae objects: individual (PKS1830–211) — galaxies : abundances — galaxies : ISM — quasars : absorption lines — gravitational lensing

## 1. Introduction

The molecular interstellar medium (ISM) in galaxies at redshifts up to  $z \approx 0.9$  has been studied through the use of absorption of molecular rotational transitions (cf. Wiklind & Combes 1996a,b; Combes & Wiklind 1995). Detection of several different lines of molecules such as CO, HCO<sup>+</sup>, HCN, HNC, CS, N<sub>2</sub>H<sup>+</sup>, H<sub>2</sub>CO, etc. allows a derivation of accurate excitation temperatures, column densities and abundance ratios (Wiklind & Combes 1994, 1995, 1996a,b). Four molecular absorption line systems are known to date; in two of them the absorption occurs in the host galaxy to the AGN and two represent truly intervening galaxies. Since the distribution of molecular gas in galaxies is usually centrally concentrated, the likelihood to encounter a molecular cloud is higher if the line of sight passes close to the center of an intervening galaxy. This means that also the likelihood for gravitational lensing is high and, indeed, in each of the two systems where absorption occurs in an intervening galaxy, that galaxy acts as a gravitational lens to the background source (Wiklind & Combes 1995, 1996a)

The use of molecular absorption lines is manifold. Apart from studying the physical and chemical properties of molecular gas in distant galaxies, they can be used as probes of very small scale structures in the molecular gas. They can also be used as cosmographic probes, to set upper limits to the temperature of the cosmic microwave background radiation and to constrain the geometry in gravitationally lensed systems. The molecular ISM is probed on a scale of a few tenths of a parsec, limited only by the angular extent of the background source. The main uncertainty in the molecular gas properties derived from the absorption lines is due to our ignorance of possible small scale structures in the ISM on scales smaller than the angular extent of the background source (e.g. Wiklind & Combes 1997).

In this article, we concentrate on the absorption line system originating in a galaxy which plays the role of a gravitational lens at  $z=0.886$  (Wiklind & Combes 1996a). The galaxy absorbs the continuum of the strong flat-spectrum radio source PKS1830–211. This radio source has long been considered a gravitational lens candidate on basis of the radio structure (Rao & Subrahmanyan 1988; Jauncey et al. 1991). Since optical and near-infrared searches for an optical counterpart to the radio source as well to the lensing

galaxy have remained unsuccessful (cf. Djorgovski et al. 1992), the modeling of the lensing system was lacking redshift information (Kochanek & Narayan 1992; Nair, Narasimha & Rao 1993). The galaxy at  $z=0.886$  was discovered by searching for molecular absorption lines in the 3- and 2-mm band (Wiklind & Combes 1996a). A second intervening system has been reported at  $z=0.193$ , seen through 21 cm HI absorption by Lovell et al. (1996).

We present new molecular absorption data on the galaxy at  $z=0.886$  as well as upper limits to molecular absorption and emission on the  $z=0.193$  system. We also discuss what can be inferred regarding the mass of the lensing galaxy and the redshift of the background source.

## 2. Observations and data reduction

Our data were obtained using the IRAM millimeter wave interferometer situated on Plateau de Bure in France, the single dish IRAM 30-m telescope on Pico Veleta in Spain and the 15-m SEST (Swedish ESO Submillimeter Telescope) on La Silla in Chile. The interferometer observations were done on several occasions during 1995 and 1996. The single dish observations were likewise obtained during several observing runs in 1995 and 1996.

At the IRAM 30-m telescope we used 3-, 2-, and 1.3-mm SIS receivers tuned to the redshifted frequency of the observed transition. The observations were made using a nutating subreflector with a frequency of 0.5 Hz and with a throw of  $\pm 90^\circ$  in azimuth. Typical system temperatures in the  $T_A^*$  scale were 400–600 K. The weather conditions were good on most observing sessions. Pointing, focusing and calibration were done before each observation. As backends we used narrow band autocorrelators, giving a velocity resolution of approximately  $0.7 \text{ km s}^{-1}$  and a bandwidth of  $400 \text{ km s}^{-1}$ . At the SEST we used 3-, and 2-mm SIS receivers with typical system temperatures 200–300 K. Here we used an AOS with a bandwidth of  $1200 \text{ km s}^{-1}$  and a velocity resolution of  $0.7 \text{ km s}^{-1}$ . These observations were done in a dual beamswitch mode, where the beam is displaced  $12'$  in azimuth at a frequency of 6 Hz. The SEST data was obtained under good weather conditions. Pointing and calibration were done as at IRAM.

The interferometer data were made with the standard BC configuration (see Guilloteau et al. 1992). The array comprised 4 15-m telescopes. The receivers

were 3-mm SIS, giving a typical system temperature of 400–500 K. PKS1830–211 itself was used as a phase reference, while bandpass and amplitude calibrations were done using also NRAO 530, 3C454.3 and W3OH. The data reduction was made with the standard CLIC software. Due to the low elevation of the PKS1830–211, we obtained a beam of 6 x 2.4 arcsec. This appears insufficient to resolve two images separated by only one arcsec; but due to the high signal-to-noise ratio, we were able to fit the integrated line profile and the phase center, as a function of frequency, directly from the visibilities. We also made a two point sources fit, which gave the relative positions of the two images and their relative fluxes.

The accuracy of the measurement depends on the inherent uncertainty in the chopper-wheel calibration method as well as the pointing of the telescope. The overall accuracy for a single observation on the intensities are around 5–10% for the interferometer data and 10–20% for the single dish data.

### 3. Results

#### 3.1. The location of the z=0.886 absorption

In our first study of the molecular absorption line system towards PKS1830–211 we found that the  $\text{HCO}^+(2\leftarrow 1)$ ,  $\text{HCN}(2\leftarrow 1)$  and, possibly, the  $\text{HNC}(2\leftarrow 1)$  lines were heavily saturated (Wiklind & Combes 1996a). Yet, the depths of these absorption lines were only 36% of the total continuum. Since the magnification ratio derived from long wavelength interferometer data is 1.8 (Nair et al. 1993), corresponding to a flux fraction of  $\sim 36\%$  for the SW and 64% for the NE core<sup>1</sup>, respectively, we concluded that the molecular gas only covers the SW core, with a high covering factor (close to 100%). The present interferometric results confirm that only the SW component is absorbed around  $V = 0$ .

In Fig. 1 we show the  $\text{HCO}^+(2\leftarrow 1)$  spectrum obtained with the Plateau de Bure interferometer. The low declination of PKS1830–211 makes imaging difficult, partly due to a north-south elongated beam, and to the large air-mass. The continuum is, however, strong enough to allow a self-calibration of the data. We made a gaussian fit of the source directly from the visibility data, and traced the location of the phase-center as a function of frequency. The accuracy is

very good in RA ( $\sim 0.05''$ ) and slightly worse in DEC ( $\sim 0.1''$ ). The two top panels in Fig. 1 show the relative phase in RA and DEC as a function of velocity across the absorption profile. From the data obtained in September and October 1995, the maximum shifts are  $\Delta\alpha = 0.22''$  and  $\Delta\delta = 0.28''$ . From the April 1996 data we get  $\Delta\alpha = 0.24''$  and  $\Delta\delta = 0.26''$  (see also Fig. 3).

If the flux fraction from the NE and SW cores are  $f_1$  and  $f_2$ , respectively ( $f_1 + f_2 = 1$ ), the shift of the phase-center along the line joining the cores is

$$\Delta\alpha = \beta(v)f_2r \sin \psi \quad , \quad \Delta\delta = \beta(v)f_2r \cos \psi \quad ,$$

where  $\beta(v)$  is the fraction of continuum flux from the SW core that is covered by optically thick molecular gas of velocity  $v$ ,  $r$  is the separation of the two components and  $\psi$  is the position angle of the line joining the two cores, measured from north to east. From the 15 GHz VLA continuum map presented by Subrahmanyan et al. (1990), we derive  $r = 0.98''$  and  $\psi = 44^\circ$ . Expressing the flux fractions in terms of the magnification ratio  $R = f_1/f_2$ , we get  $\beta = (1 + R)\Delta\alpha/(r \sin \psi)$ . Using the magnification ratio  $R$  derived from long wavelength interferometry of 1.8 (Nair et al. 1993) and assuming that the covering factor  $\beta$  is 100% for the SW component, the phase-center should shift  $\Delta\alpha \approx 0.24''$  and  $\Delta\delta \approx 0.25''$ , which is consistent with the shift that we see in Fig. 1.

Frye, Welch & Broadhurst (1997) observed PKS1830–211 with the BIMA interferometer and derived a magnification ratio of  $1.14 \pm 0.05$  by resolving the two continuum components. Since the  $\text{HCO}^+(2\leftarrow 1)$  line is manifestly optically thick, as seen through the detection of the  $\text{H}^{13}\text{CO}^+(2\leftarrow 1)$  line (Wiklind & Combes 1996a), such a low magnification ratio indicates that the covering factor  $\beta$  of the SW core is only 80–84%. However, they measure a total flux of 2.25 Jy in March 96 (1 March and 20 March), much larger than ours of  $1.55 \pm 0.06$  Jy on 28 February and  $1.45 \pm 0.08$  Jy on 14 April 96). Measurements made with the Owens Valley interferometer on 1 March gave  $1.6 \pm 0.1$  Jy (S. Aalto priv. comm.). It thus appears that the continuum is overestimated by a factor 1.4–1.5 in Frye et al. (1997). We stress that calibration is quite delicate since there exist significant rapid variations in the continuum levels of the two images. Given the high signal-to-noise of the Plateau de Bure observations, we have tried to retrieve the magnification ratio from a two point sources fit of the visibility data. The fits

<sup>1</sup>Henceforth we refer to the north-east component as NE and the south-west component as SW.

were very robust, completely independent of the initial parameters, and revealed an RA and DEC separation between the two images exactly consistent with  $r = 0.98''$  and  $\psi = 44^\circ$  in all the 136 channels without absorption. In Table 1 we show the magnification ratios obtained at the various epochs. Although the absolute calibration is not so precise, we believe that the relative ratios between the two components is accurate. Although the magnification ratio has changed from  $1.8 \pm 0.1$  to  $1.2 \pm 0.1$  between October 1995 and April 1996, in concordance with the value derived by Frye et al, the lower continuum level measured by us is in agreement with a covering factor  $\sim 1$  for the SW component (see Sect. 4.2).

### 3.2. A second absorbing cloud at $z=0.88489$

We have detected a second absorption component situated at a velocity  $-147 \text{ km s}^{-1}$  relative to the main  $\text{HCO}^+(2\leftarrow 1)$  absorption at  $z=0.88582$ . The second component is hereafter referred to as the ‘satellite’. The  $\text{HCO}^+(2\leftarrow 1)$  line has been observed extensively during a monitoring campaign at both the IRAM 30-m and SEST 15-m telescope. Averages of data obtained during 1996 are shown in Fig. 2, where the two dashed vertical lines mark zero velocity and  $-147 \text{ km s}^{-1}$  in a heliocentric velocity scale in the restframe of the  $z=0.88582$  absorber. The satellite line is not seen in the  $\text{HCO}^+(3\leftarrow 2)$  spectrum. Frye et al (1997) could have detected this component in March 96 (since the line was present at this epoch, see Fig. 3), but their lower signal-to noise ratio prevented the detection.

Could the second absorption line be associated with the  $z=0.193$  HI absorber rather than the one at  $z=0.886$ ? The only line at  $z=0.193$  which could be in the ‘vicinity’ of the observed frequency of the satellite line at  $94.635 \text{ GHz}$  is the redshifted  $\text{CO}(1-0)$  line at  $96.650 \text{ GHz}$ . The difference is in excess of  $2 \text{ GHz}$ , corresponding to a velocity difference of  $\sim 6200 \text{ km s}^{-1}$  in the restframe of the  $z=0.193$  absorber. It is therefore highly unlikely that the satellite absorption is associated with this system. We conclude that the satellite line is a second  $\text{HCO}^+(2\leftarrow 1)$  line at a blueshifted velocity of  $-147 \text{ km s}^{-1}$  relative to the redshift  $z=0.88582$  (corresponding to a redshift of  $z=0.884896 \pm 0.00001$ ).

Whereas the main absorption line at  $V = 0$  has a depth of 38–40% of the total continuum, the satellite line has a depth of only 7%. Measured in antenna temperature, this corresponds to  $1.5 \text{ mK}$  and  $6 \text{ mK}$  in

the SEST and IRAM data, as of April 96. The actual opacity, however, depends on the surface covering factor of the absorption. The separation of the NE and SW continuum components is  $0.98''$ , corresponding to a distance of  $5.6 \text{ kpc}$ , measured in the plane of the sky ( $H_0 = 75 \text{ km s}^{-1} \text{ Mpc}^{-1}$ ,  $q_0=0.5$ ). The satellite absorption can therefore be associated with only one of the continuum sources. Since the flux contribution from the NE and SW components are  $\sim 60\%$  and  $\sim 40\%$ , respectively, the satellite absorption line is either optically thin or has a very small covering factor.

The satellite absorption line is clearly seen in the interferometer data (Fig. 3). The relative location of the phase-center for  $\Delta\alpha$  is shown in the top panel. In addition to the positive shift of the phase-center already established for the main absorption around  $V = 0 \text{ km s}^{-1}$ , a shift is also seen at the velocity of the satellite line, but this time towards negative values. This shows that the phase-center moves partly towards the SW continuum component at the velocity of the satellite absorption. The second absorption component must therefore originate in front of the NE continuum core. We are thus seeing molecular gas from two different parts of the intervening galaxy.

Two absorption components, separated by  $330 \text{ km s}^{-1}$ , are also seen at  $z=0.673$  towards the radio source B3 1504+377 (Wiklind & Combes 1996b). In this case the absorption occurs in the galaxy hosting the radio source. The galaxy is close to edge-on and the separation of the two absorption lines are caused by non-circular velocities along a single line of sight within the disk of the host galaxy, most likely caused by the presence of a barred potential. The line of sight to the two images of the continuum core of PKS1830-211 passes through the intervening galaxy at  $\sim 1.8$  and  $\sim 3.8 \text{ kpc}$  (SW and NE components) from the lens center (Nair et al. 1993). A normal rotation curve (and circular orbits) are sufficient here to account for the observations.

We derived column densities using the formalism presented in Wiklind & Combes (1995, 1997). The  $\text{HCO}^+$  column density of the satellite absorber, derived using 60% of the total flux, is only  $7 \times 10^{12} \text{ cm}^{-2}$  (however we can not exclude the case of a highly saturated line with a small covering factor). Using 40% of the total flux for the main line, we find an  $\text{HCO}^+$  column density  $> 5 \times 10^{14} \text{ cm}^{-2}$ . This value is derived from the averaged monitoring data for 1996 and is slightly higher than the column density reported in Wiklind & Combes (1996a). Since the main line is

heavily saturated, the difference is due to the much better signal-to-noise ratio of the new data. The column densities have been derived using an excitation temperature  $T_x = 6$  K. Integrating the J=3←2 spectrum over the extent of the J=2←1 line sets a  $3\sigma$  upper limit to the excitation temperature of 8 K (a  $2\sigma$  limit implies  $T_x < 6$  K).

### 3.3. The z=0.193 21 cm HI absorber

We searched for redshifted CO(1←0) absorption and/or emission as well as HCO<sup>+</sup>(2←1) absorption at z=0.19267. Neither emission nor absorption was found. The CO and HCO<sup>+</sup> spectra are shown in Fig. 4.

#### 3.3.1. Limits to the CO and HCO<sup>+</sup> column densities

The continuum level at the redshifted frequency of the CO(1←0) and HCO<sup>+</sup>(2←1) lines are 50 mK and 26 mK, at the SEST telescope. However, when deriving upper limits to the column density for molecular absorption we have to take the separate flux contributions into account. While the 21 cm HI absorption only occurs over the NE component (Lovell et al. 1996), putative molecular absorption can occur in front of both components. In Table 2 we give upper limits for three cases; (1) the total continuum flux, (2) 60% of the flux, corresponding to the NE component, and (3) 40%, corresponding to the SW component. In all cases we assume an excitation temperature of 6 K. The ratio of the upper limits of the molecular column density to that of the HI is done for the NE component, since this line of sight causes the atomic absorption at z=0.193.

We derived the HI column density from the spectra presented in Lovell et al. (1996), by fitting two gaussian profiles. The resulting column density is  $N_{\text{HI}} = 1.5 \times 10^{18} T_{\text{sp}} / f \text{ cm}^{-2}$ , where  $T_{\text{sp}}$  is the spin temperature and  $f$  is the area filling factor. Since the HI absorption is only seen towards the NE component  $f = 0.6 f'$ , where the factor 0.6 corresponds to the flux contribution of the NE component and  $f'$  is the area covering factor of atomic gas for this component. Assuming a spin temperature of 100 K, which is typical for atomic hydrogen gas in the Milky Way, the column density of atomic gas is  $2.5 \times 10^{20} f'^{-1} \text{ cm}^{-2}$ . For the abundance ratios given in Table 1 we set  $f' = 1$ .

Using a typical value for  $N(\text{H}_2)/N(\text{CO})$  of  $10^4$ , the abundance ratio of molecular and atomic hydrogen is  $< 0.25$  in the z=0.193 absorber. This limit is not very

illuminating, since the column density of atomic gas is relatively low, corresponding to an extinction  $A_V \approx 0.16$  mag (e.g. Savage et al. 1977). Since CO becomes self-shielded only at  $A_V \gtrsim 1$  mag (e.g. Lucas & Liszt 1994) we do not expect a significant amount CO at these low HI column densities. Molecular hydrogen, however, can still be present, since it becomes self-shielded at lower  $N_{\text{HI}}$ .

#### 3.3.2. Limits to $M_{\text{H}_2}$ from CO emission

Our CO(1←0) spectra of the z=0.193 HI absorption can also be used to derive an upper limit to the global molecular mass content of any intervening galaxy at this distance. The single dish telescope beam has a FWHM size of  $52''$  at a frequency of 96.65 GHz, corresponding to  $\sim 143$  kpc at z=0.193. Since atomic gas disks are considerably smaller than this, an intervening galaxy causing the 21 cm HI absorption at z=0.193 must be within our telescope beam. The effective beam of the interferometer data is  $6'' \times 2.4''$  ( $16.5 \times 6.6$  kpc) with a noise rms of 10 mJy/beam. The field of view is the same as for the single dish observation, since 15-m telescopes were used in both cases.

The single dish CO spectrum shown in Fig. 4 has a channel-to-channel noise rms of 1.0 mK when binned to a resolution of  $17 \text{ km s}^{-1}$ . No emission is evident in the spectrum and we derive a  $3\sigma$  upper limit to the integrated CO intensity by assuming a linewidth of  $200 \text{ km s}^{-1}$  to be  $< 0.17 \text{ K km s}^{-1}$ . The CO(1←0) spectrum does have a high frequency baseline curvature, which has been removed in the spectrum shown in Fig. 4. The uncertainty in the derived integrated intensity is limited by this curvature, but only for emission more extended than  $1000 \text{ km s}^{-1}$ . Since such wide emission profiles are rarely encountered, we believe that the baseline curvature is of little concern in this case. The interferometer data does not suffer from any baseline curvature and gives a  $3\sigma$  upper limit to the integrated CO intensity of  $< 0.09 \text{ K km s}^{-1}$

The CO line luminosity, expressed in  $\text{K km s}^{-1} \text{ pc}^2$ , can be written as

$$L'_{\text{CO}} = \Omega_{s*b} D_L^2 \frac{I_{\text{CO}}}{(1+z)^3} \text{ K km s}^{-1} \text{ pc}^2, \quad (1)$$

where  $D_L$  is the luminosity distance,  $I_{\text{CO}}$  is the velocity integrated CO intensity expressed in  $\text{K km s}^{-1}$ , and  $\Omega_{s*b}$  is the solid angle of the source brightness distribution convolved with the telescope beam,  $\Omega_b$ . For distant sources and single dish telescopes, this convolution is dominated by the solid angle of the beam and

we can approximate it with  $\Omega_{s*b} \approx \Omega_b \approx 26.56 \times B^2$ , (e.g. Solomon et al. 1997), where  $B$  is the full width at half power of the telescope beam measured in arc-seconds<sup>2</sup>. The mass of molecular gas is obtained by assuming a conversion factor between CO luminosity and the column density of H<sub>2</sub>:  $M_{\text{H}_2} = \alpha L'_{\text{CO}}$ . We use a standard Milky Way conversion factor  $\alpha = 4.6 M_{\odot} (\text{K km s}^{-1} \text{ pc}^2)^{-1}$  (e.g. Solomon et al. 1997). With these values our upper limits to  $I_{\text{CO}}$  transform into a  $3\sigma$  upper limit to the H<sub>2</sub> mass of  $5 \times 10^9 M_{\odot}$  and  $2.5 \times 10^9 M_{\odot}$  for the single dish and interferometer data, respectively.

### 3.4. Additional absorption lines

In addition to the 12 absorption lines presented in Wiklind & Combes (1996a) we have detected additional absorption lines from CO(4←3), H<sub>2</sub>CO(2<sub>11</sub> ← 1<sub>01</sub>) and H<sup>13</sup>CN(2←1). The spectra are presented in Fig. 5 together with a new spectra of H<sup>13</sup>CO<sup>+</sup>(2←1) obtained with the IRAM 30-m telescope.

For the first time we detect one of the CO lines in this system. The redshift of the absorber is such that the three first rotational transitions of CO fall at frequencies unfavorable for ground based observations. The CO(4←3) line, however, is shifted into the 1-mm band. We observed this line with the IRAM 30-m telescope in May 1996 and the spectrum is presented in Fig. 5a. The line is rather strong, with a depth almost equal to that of the saturated transitions of HCO<sup>+</sup> and HCN. Using 40% of the total flux and an excitation temperature of 6 K, the CO column density is  $2 \times 10^{18} \text{ cm}^{-2}$ . Should  $T_x$  be higher, say 20 K, the column density becomes  $0.2 \times 10^{18} \text{ cm}^{-2}$ . For higher excitation temperatures the column density increases again. The main uncertainty in this derivation is the continuum flux. Due to unstable weather conditions it was not possible to derive  $T_c$ . We have used the continuum flux determined from the 3- and 2-mm bands, which corresponds to 1.2 Jy and converted this to antenna temperature in the 1-mm band. Although indirect, the energy distribution of the radio source PKS1830-211 is flat enough to make this approach viable. The excitation temperature of CO can be higher than the low values found for HCO<sup>+</sup>, HCN, N<sub>2</sub>H<sup>+</sup>, CS, etc. (see Wiklind & Combes 1996a). The reason is the lower electric

dipole moment of CO, making it more easily collisionally excited and giving CO a higher level population at rotational levels  $J \geq 3$  than do HCO<sup>+</sup> and HCN. Different excitation temperatures for CO and the other molecular species is consistent with the ‘weak LTE’ conditions assumed when deriving the excitation temperature, where it is assumed that the level population of each molecule is characterized by a unique temperature (that is:  $T_x = T_{\text{rot}}$ ), but this temperature can be different from one molecular species to another (see Wiklind & Combes 1995, 1997).

We also report the detection of ortho-H<sub>2</sub>CO through the  $J_{K_a K_b} = 2_{11} \leftarrow 1_{01}$  line (Fig. 5b). The line appears to be non-saturated with a maximum optical depth  $\sim 1$ . The column density of ortho-H<sub>2</sub>CO is  $2 \times 10^{15} \text{ cm}^{-2}$ , assuming  $T_x = 6 \text{ K}$  and a flux fraction of 40%.

Absorption of H<sup>13</sup>CO<sup>+</sup> was reported already in Wiklind & Combes (1996a), but the present spectra represents a significant improvement to the signal-to-noise. The detection of this isotopic species was one of the main arguments in favor of a high H<sup>12</sup>CO<sup>+</sup>(2←1) line opacity. The column density of H<sup>13</sup>CO<sup>+</sup>, derived assuming the same excitation temperature as for the main isotope of 6 K, is  $2 \times 10^{13} \text{ cm}^{-2}$ . The H<sup>12</sup>CO<sup>+</sup>/H<sup>13</sup>CO<sup>+</sup> ratio is thus  $> 25$ , possibly much higher. From the similar absorption depth of HCO<sup>+</sup>(2←1) and HCN(2←1) we inferred that also the HCN line was heavily saturated (Wiklind & Combes 1996a). This is confirmed by the detection of the H<sup>13</sup>CN(2←1) line with the IRAM 30-m telescope (Fig. 5d). The column density of H<sup>13</sup>CN is  $6 \times 10^{12} \text{ cm}^{-2}$  (again using 40% of the total flux and adopting an excitation temperature of 6 K). The H<sup>12</sup>CN/H<sup>13</sup>CN ratio is  $> 50$ .

## 4. Discussion

### 4.1. The lensing galaxy at $z=0.886$

The detection of a second absorption line component at a redshift  $z=0.886$ , shifted in velocity relative to the main one and associated with the NE image of the background source, opens up a unique possibility to derive the dynamical mass of the central few kpc of the lensing galaxy. This is valuable information when modelling the lens, specifically when using time delay measurements to derive cosmographic parameters such as the Hubble constant. At the present this is hampered by the non-detection of the lensing galaxy at optical and infrared wavelengths (e.g. Djorgovski et al. 1992). This is likely to change with new and

<sup>2</sup>Solomon et al. (1997) do not take the gaussian shape of the telescope beam into account and their molecular mass formula therefore gives a 13% lower mass estimate.

more powerful infrared detectors.

It is, however, possible to use very simple but powerful arguments, based on the assumption that the lensing galaxy is a ‘normal’ disk galaxy, to get reasonable ranges for the mass of the lensing galaxy as well as the redshift of the background radio source already from the present data.

The observed line of sight velocity in a disk galaxy of inclination  $i$ , having a rotational velocity  $V(R)$  is

$$V_{\text{obs}} = V(R) \cos \theta \sin i ,$$

where  $R$  is the galactocentric radius in the plane of the galaxy and  $\theta$  is the angle from the line of nodes, as measured in the plane of the galaxy.  $R$  and  $\theta$  are related to the radius  $r$  and angle  $\phi$  measured in the plane of the sky through

$$R = r \left( \cos^2 \phi + \frac{\sin^2 \phi}{\cos^2 i} \right)^{1/2} , \quad \tan \phi = \tan \theta \cos i .$$

If we assume (it will be justified below) that  $i$  is small (i.e.  $i \lesssim 30^\circ$ ), the differences between radii and angles measured in the plane of the sky and those in the plane of the galaxy are small ( $\cos i \gtrsim 0.87$ ). This is a reasonable assumption since, as we will show below, the dynamical mass required to cause the image separation of PKS1830–211 implies that the rotational velocity of the lensing galaxy is more than twice larger than the observed velocity separation of the main and satellite absorption lines (e.g.  $\sin i < 0.5$ , and  $i < 30^\circ$ ). If we also make the assumption that the rotation curve is similar in shape to those found in nearby galaxies, we can assert that the rotational velocity is approximately constant at radii  $\gtrsim 2$  kpc. This is seen from inspection of the rotation curves derived for all different types of spiral galaxies by Rubin et al. (1980, 1982, 1985). Two different lens models have been produced for PKS1830–211 (Kochanek & Narayan 1992; Nair et al. 1993). They both agree that the center of the lensing galaxy is close to the center of the ring seen in radio interferometer data and that the lens has a small eccentricity. The model of Nair et al. places the center of the lens somewhat closer to the SW image than that of Kochanek & Narayan. In the former case the SW and NE cores are seen at projected distances of 1.8 kpc and 3.8 kpc from the center. In the model by Kochanek & Narayan, both cores are  $\sim 3$  kpc from the center of the lens. In either case, it is reasonable to assume that the rotational velocity of the lensing galaxy has reached a

relatively constant value at the projected location of both the SW and NE cores;  $V(R) \approx V_0$ . The observed velocity difference between two points in the galaxy is then

$$\Delta V_{\text{obs}} = V_0 (\cos \theta_1 - \cos \theta_2) \sin i ,$$

where  $\theta_j$  is the angle between the line of nodes and the line joining the center of the lens with the point where the line of sight crosses the disk, measured east of north.

The angles  $\theta_j$  are  $52^\circ$  and  $204^\circ$  for the NE and SW components, respectively. This gives a simple relation between the maximum velocity  $V_0$ , the inclination  $i$  and the observed velocity separation of the absorption lines:  $|\Delta V| = V_0(1.5 \cos \psi + 1.2 \sin \psi) \sin i$ , where  $\psi$  is the position angle of the major axis of the lensing galaxy. Geometrical considerations of the lensing morphology implies that the position angle is either  $\sim 0^\circ$  or  $\sim 90^\circ$  (Kochanek & Narayan 1992; Nair et al. 1993). The mass inside a radius  $R$  is given by the virial theorem

$$M(< R) \approx \frac{\Delta V^2 R}{\beta^2 G \sin^2 i} \approx \frac{7 \times 10^9}{\sin^2 i} M_\odot ,$$

where  $\beta$  is the factor depending on the position angle of the lens:  $\beta = 1.5$  for  $\psi = 0^\circ$  and  $\beta = 1.2$  for  $\psi = 90^\circ$ . We will adopt a position angle  $\psi = 0^\circ$  in the following, keeping in mind that values can change by at most 20% should the position angle be  $90^\circ$ . In the last equality we used  $\Delta V = 147 \text{ km s}^{-1}$  and  $R = 3$  kpc.

The two radio-components in PKS1830–211 have almost identical substructure, suggesting that the components are two parity-reversed images of the background quasar caused by a nearly perfect alignment of the lens and the source (e.g. Nair et al. 1993). The separation of the NE and SW images can therefore to first order be described as the effect of a single point mass deflector of mass  $M$ , with the image separation given by the ‘Einstein angle’  $\Delta\theta_E$

$$\Delta\theta_E = 4 \sqrt{\frac{GM}{c^2 D}} \approx 5.7 \times 10^{-6} \sqrt{\frac{M}{D}} \text{ arcseconds} .$$

In the last equality  $M$  is expressed in solar mass and the distance parameter  $D$  in Gpc;  $D = D_d D_s / D_{\text{ds}}$ , where  $D_d$  is the distance between the observer and the lens,  $D_s$  the distance between observer and the source, and  $D_{\text{ds}}$  the distance between the lens and the source, all measured as angular size distances (e.g.

Schneider, Ehlers & Falco 1992). The last equation yields:

$$M \approx 3 \times 10^{10} D M_{\odot},$$

( $D$  in Gpc), and with the virial theorem:

$$V_0 \approx 220\sqrt{D} \text{ km s}^{-1}, \quad (2)$$

In Fig. 6 we plot  $D$  as a function of the source redshift for a fixed lens redshift of  $z=0.88582$ . The distances are derived using  $H_0 = 75 \text{ km s}^{-1} \text{ Mpc}^{-1}$  and for  $q_0 = 0.5$  (full-drawn line) and  $q_0 = 0.05$  (dotted line).  $D$  remains larger than 2 for all source redshift less than  $z \approx 7$ . This, together with the last equation, means simply that the observed image separation of  $\sim 1''$  already requires a massive galaxy for the lens: for a redshift of the background source  $\gtrsim 3$ , the required rotational velocity is  $350 \text{ km s}^{-1}$ , corresponding to a massive early type spiral. Lower redshifts for the background source would require higher rotational velocities, corresponding to an even more massive galaxy, which is not realistic for spirals (unless several galaxies are considered to contribute to the lensing). Rotational velocities typical for late type spirals can be excluded, since the redshift of the background source becomes forbiddingly large. Now, using the relation  $\Delta V = 1.5V_0 \sin i$  derived above, with  $\Delta V = 147 \text{ km s}^{-1}$  and  $V_0 = 350 \text{ km s}^{-1}$ , yields an inclination of  $i = 16^\circ$ .

How sensitively do these conclusions depend on the assumptions? (1) The approximation of the lensing mass as a singular point mass is only correct to first order if the lens and the background source are aligned. This is approximately true for PKS1830–211. (2) The derivation of inclination assumes that the absorbing gas is on circular orbits. If it has non-circular motion with an amplitude comparable to the rotational velocity, this simple approach is not valid. However, the lens model of Kochanek & Narayan (1993) independently finds a low inclination. (3) The presence of an absorber at  $z=0.193$  introduces extra shear and, possibly, convergence of the ray bundles. However, given the relatively simple image configuration it is not likely that the extra mass concentration at low redshift adds to the image multiplicity. It can, however, influence the interpretation of time delay measurements and Garrett et al. (1996) find from VLBI observations that the NE core component has a more extended and complex morphology than the SW component, which could be caused by the extra mass at  $z=0.193$ . Hence, our results regarding the mass of

the lens at  $z=0.886$  and the lower limit to the redshift of the source are quite robust and we can make the following postulates:

1. the lensing galaxy is an early type spiral galaxy seen at a low inclination ( $i < 20^\circ$ ).
2. The mass within a radius of  $\sim 3 \text{ kpc}$  is in the range  $\sim 6-9 \times 10^{10} M_{\odot}$ , which is similar, within a factor 2, to the Milky Way galaxy.
3. The redshift of the background source is large, most likely  $z_s > 3$ .

#### 4.2. The covering factor of the SW component

Frye et al. (1997) observed PKS1830–211 with the BIMA millimeter array and found  $\text{HCO}^+(2\leftarrow 1)$  absorption only over the SW component, as we do. However, the absorption line over this region did not reach zero level, indicating a filling factor of 70-80%. This would mean that the prospect of using single dish instruments to monitor the continuum and depth of saturated absorption lines with the aim of deriving the time delay between the NE and SW components can lead to ambiguities. However, interferometric imaging of an object at low elevations is difficult in the millimeter band and it is unclear how the accuracy of the interferometer data can be assessed. The flux ratio between the NE and SW continuum components in the BIMA data is  $1.14 \pm 0.05^3$  (Frye et al. 1997), compatible with our value at the same epoch, but their total flux is much higher than what we find, either with Plateau de Bure, IRAM–30m or SEST. In any case, the covering factor is quite high, almost 1 for our measurements (see Table 1), and is also compatible within 1 for the data of Frye et al (1997) when their noise level is taken into account or if their continuum level is overestimated by a factor  $\sim 1.4$ . We do not think that this uncertainty is the main one in the time-delay determination, the major uncertainty being the continuum level measurement.

It is not unexpected that a molecular cloud covers entirely one of the PKS1830–211 image. The angular extent of the continuum emission region in the millimeter regime is not well known. The SW image remains unresolved in 15 GHz VLBA observations (Garrett et al. 1996) at a resolution of

<sup>3</sup>Taking the quoted fluxes and errors from Frye et al. (1997), we get a flux ratio of  $1.14 \pm 0.24$ .



$0.6 \times 0.2$  milliarcseconds (mas). The NE component, however, is resolved with a complex structure. An angular extent of 0.2 mas corresponds to  $\sim 1.1$  pc but the size of the continuum source at millimeter wavelengths can be considerably smaller. Millimeter VLBI of the BL Lac 3C446 found an upper limit to the angular extent of  $30 \mu\text{arcseconds}$  (Lerner et al. 1993).

In Fig. 7 we show the spectrum of the  $\text{HCO}^+(2\leftarrow 1)$  absorption obtained with the Plateau de Bure interferometer with a velocity resolution of  $0.5 \text{ km s}^{-1}$ . The profile is asymmetric with an extension towards negative velocities. This part of the profile is either optically thin or has a covering factor less than the narrow component. Saturated absorption lines of a finite width should be flat-bottomed when viewed with a high velocity resolution. The bottom of the narrow profile shown in Fig. 7 appears to be deeper at negative velocities than at positive. The effect is only at the 1-2% level. However, a similar asymmetry is seen in the lower resolution  $\text{HCO}^+(2\leftarrow 1)$  spectra obtained from both the IRAM 30-m and SEST telescopes (Fig. 2). This asymmetry could represent small differences in the covering factor of the saturated absorption, corresponding to linear dimensions of  $\sim 5\%$  of the extent of the continuum source.

## 5. Summary

We have reported further molecular lines in absorption towards PKS1830-211, and in particular  $\text{CO}(4\leftarrow 3)$ , the first CO line. Molecular abundances are compatible with Milky Way values.

We have also carried out interferometric measurements at three different epochs, and found that the magnification ratio between the two images has decreased from 1.8 to 1.0 during one year. These measurements confirm that the main  $V=0$  absorbing component covers the SW image. We report about the detection of a second component at  $V=-147.5 \text{ km s}^{-1}$ , which covers only the NE image.

The presence of two absorption lines, one corresponding to the SW image of the background source and the other to the NE component, implies that the background radio source is situated at a redshift  $\gtrsim 3$ , and is consistent with the lensing galaxy being an early type spiral seen almost face-on ( $i \lesssim 16^\circ$ ). A first determination of the time delay of  $44 \pm 9$  days has been reported by van Ommen et al. (1995). Given the model dependence of this measurement, it will be quite useful to try other independent determinations

at various frequencies. We confirm here that with the SW component being nearly completely absorbed at 3mm, single dish measurements are rapid and effective for this experiment. It will however be necessary to confirm from time to time that the filling factor is still  $\approx 1$  through interferometric measurement (but this has not varied in the past year).

The lens geometry could be made more complex by the presence of another galaxy on the line of sight, detected by HI absorption by Lovell et al (1996) at  $z=0.1927$ . We detect neither molecular absorption nor emission at this redshift; the galaxy might not be exactly aligned with the quasar, which would minimise its lensing effect. Alternatively, since the HI absorption is seen only towards the NE image, and molecular absorption has now been detected towards this component also, this  $z=0.1927$  absorption could be re-interpreted as the absorption of a heavier molecule at  $z=0.88489$ , the measured molecular redshift towards this NE component. Exactly coinciding with this frequency we find the  $(7-1,0,7,6)$  transition of the PS molecule, in a low enough excitation state. This interpretation is not likely, however, due to the expected low abundance of PS in the ISM.

We thank the staff at SEST and IRAM (both at the 30-m telescope and at the Plateau de Bure interferometer) for efficient help and support during these observations. TW acknowledges support from NFR (the Swedish Natural Science Research Council) for this research and the European Southern Observatory for hospitality during a Visitor Grant Programme in Santiago.

## REFERENCES

- Combes, F., Wiklind, T. 1997, ApJ 486, L79
- Combes, F., & Wiklind, T. 1995, A&A 303, L61
- Djorgovski, S., Meylan, G., Klemola, A., Thompson, D.J., Weir, W.N., Swarup, G., Rao A.P., Subrahmanyam, R., & Smette, A. 1992, MNRAS 257, 240
- Frye, B., Welch, W.J., & Broadhurst, T. 1997, ApJ 478, L25
- Garrett, M.A., Nair, S., Porcas, R.W., & Patnaik, A.R. 1996 in IAU Symp. 173 "Astrophysical Applications of Gravitational Lensing", eds. C.S. Kochanek & J.N. Hewitt, Kluwer Pub., p. 189
- Guilloteau, S., et al. 1992, A&A 262, 624
- Jauncey, D.L. et al. 1991, Nature 352, 132
- Kochanek, C.S., & Narayan, R. 1992, ApJ 401, 461
- Lerner, M., et al., 1993, A&A 280, L117
- Lovell, J.E.J., et al. 1996, ApJ 472, L5
- Lucas, R., & Liszt, H.S. 1994, A&A 282, L5
- Nair, S., Narasimha, D., & Rao, A.P. 1993, ApJ 407, 46
- Rao, A., & Subrahmanyam, R. 1988, MNRAS 231, 229
- Rubin, V.C., Burstein, D., Ford, W.K., & Thonnard, N. 1985, ApJ 289, 81
- Rubin, V.C., Ford, W.K., Thonnard, N., & Burstein, D. 1982, ApJ 261, 439
- Rubin, V.C., Ford, W.K., & Thonnard, N. 1980, ApJ 238, 471
- Savage, B.D., Bohlin, R.C., Drake, J.F., & Budich, W. 1977, ApJ 216, 291
- Schneider, P., Ehlers, J., & Falco, E.E. 1992, Gravitational Lenses, Springer Verlag
- Solomon, P.M., Downes, D., Radford, S.J.E., & Barrett, J.W. 1997, ApJ 478, 144
- Subrahmanyam, R., Narasimha, D., Rao, A.P., & Swarup, G. 1990, MNRAS 246, 263
- van Ommen, T.D., Jones, D.L., Preston, R.A., & Jauncey, D.L. 1995, ApJ 444, 561
- Wiklind, T., & Combes, F. 1997, in press, astro-ph/9708051
- Wiklind, T., & Combes, F. 1996b, A&A 315, 86
- Wiklind, T., & Combes, F. 1996a, Nature 379, 139
- Wiklind, T., & Combes, F. 1995, A&A 299, 382
- Wiklind, T., & Combes, F. 1994, A&A 286, L9

---

This 2-column preprint was prepared with the AAS L<sup>A</sup>T<sub>E</sub>X macros v4.0.

TABLE 1  
MAGNIFICATION RATIOS AT DIFFERENT EPOCHS

Date	Total Flux	NE/SW Ratio	$\beta_{max}$ <sup>a</sup>
Oct 95	1.5	$1.8 \pm 0.1$	1.
Apr 96	1.45	$1.2 \pm 0.1$	0.9
Sep 96	0.93	$1.0 \pm 0.1$	1.

<sup>a</sup>The maximum covering factor of the SW component.

TABLE 2  
NON-DETECTION OF ABSORPTION AT  $z=0.19267$

Molecule	Transition	$\nu_{\text{rest}}^{\text{a}}$	$\nu_{\text{obs}}^{\text{b}}$	$T_{\text{cont}}^{\text{c}}$	$N_{\text{tot}} [\text{cm}^{-2}]$			$N/N_{\text{HI}}^{\text{d}}$
		GHz	GHz	mK	100%	60%	40%	
CO	1 $\leftarrow$ 0	115.271204	96.650	50	$< 3 \times 10^{15}$	$< 6 \times 10^{15}$	$< 1 \times 10^{16}$	$< 2 \times 10^{-5}$
HCO <sup>+</sup>	2 $\leftarrow$ 1	178.375065	149.559	26	$< 3 \times 10^{12}$	$< 5 \times 10^{12}$	$< 8 \times 10^{12}$	$< 2 \times 10^{-8}$

<sup>a</sup>The rest-frequency of the observed molecules taken from Lovas (1992).

<sup>b</sup>Derived from  $\nu_{\text{obs}} = \nu_{\text{rest}} / (1 + z_{\text{a}})$ .

<sup>c</sup>Continuum level measured in  $T_{\text{A}}^*$ .

<sup>d</sup>Ratio of molecular column density and HI (see text for details).

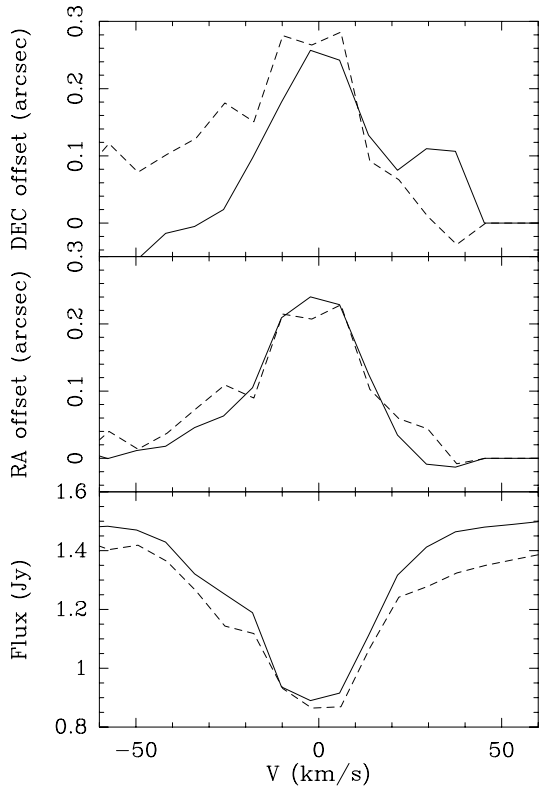


Fig. 1.—  $\text{HCO}^+(2\leftarrow 1)$  spectra (bottom) obtained with the IRAM Plateau de Bure interferometer in September–October 1995 (dashed line) and April 1996 (full line). The velocity resolution is  $7.9 \text{ km s}^{-1}$  in both cases. Also shown is the relative location of the phase-center in RA and DEC (top and middle).

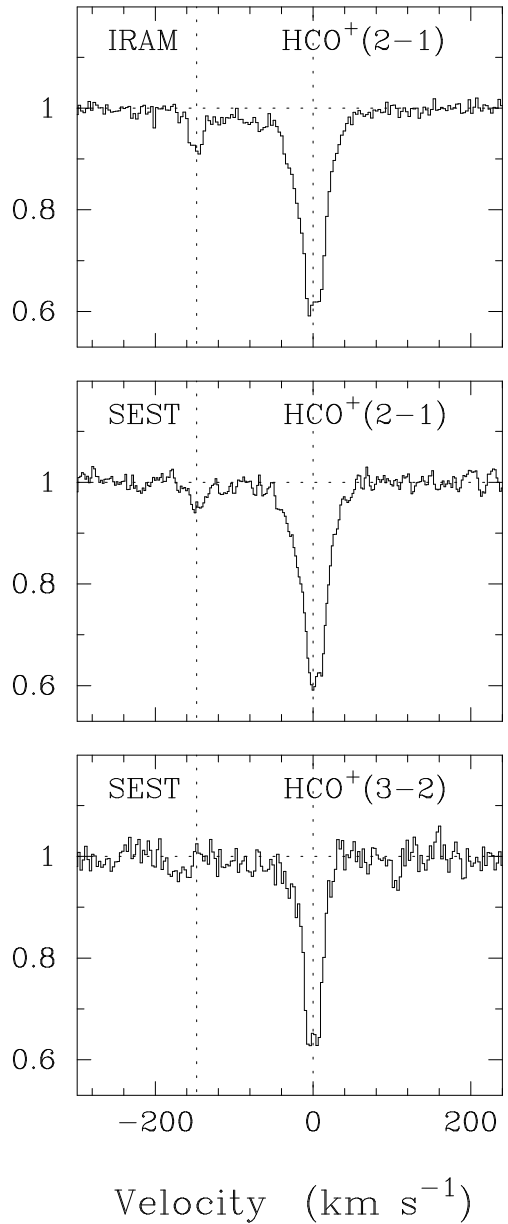


Fig. 2.— The  $\text{HCO}^+(2\leftarrow 1)$  absorption profile from the 30-m IRAM (top) and the 15-m SEST (middle) telescopes, showing the second absorption component at  $-147.5 \text{ km s}^{-1}$ . The continuum level has been normalized to unity. The vertical dotted lines mark velocities at  $-147.5 \text{ km s}^{-1}$  and  $0 \text{ km s}^{-1}$ . In the bottom, we show the  $\text{HCO}^+(3\leftarrow 2)$  spectrum, obtained with the SEST. No line at  $-147.5 \text{ km s}^{-1}$  can be seen in the  $J=3-2$  line. The velocity resolution is 3.2, 2.2 and  $2.9 \text{ km s}^{-1}$  from top to bottom.

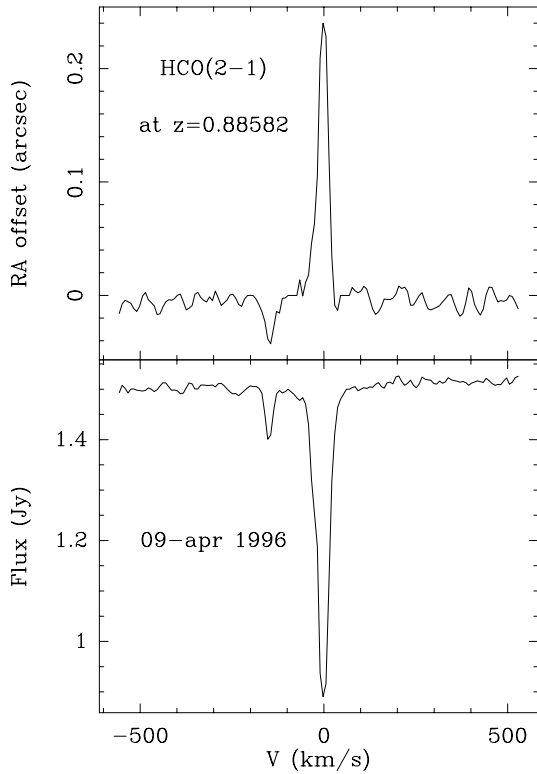


Fig. 3.— Results of the fit of visibility data from April 1996 observations: the integrated spectrum is at bottom, and the phase-center position in right ascension at top: this shows that the  $V = -147.5 \text{ km s}^{-1}$  component is absorbed in front of the NE image.

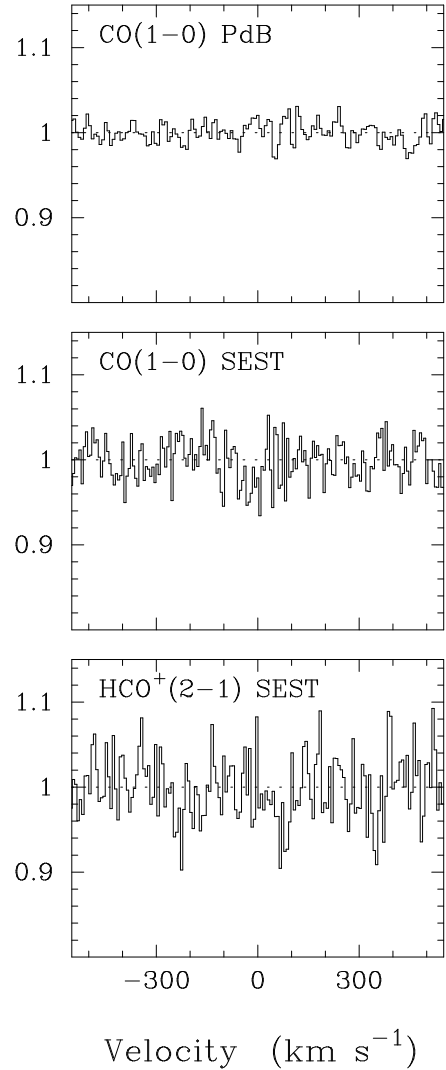


Fig. 4.— The CO(1-0) and HCO<sup>+</sup>(2-1) spectra from the  $z=0.19267$  HI absorption system. No absorption, nor emission is present. The velocity resolution is  $7.8$  and  $10.5 \text{ km s}^{-1}$  for the CO spectra and  $11.1 \text{ km s}^{-1}$  for HCO<sup>+</sup>. The velocity scale is heliocentric and the SEST spectra have been normalized to the continuum levels of  $50 \text{ mK}$  and  $26 \text{ mK}$  for CO and HCO<sup>+</sup>, respectively.

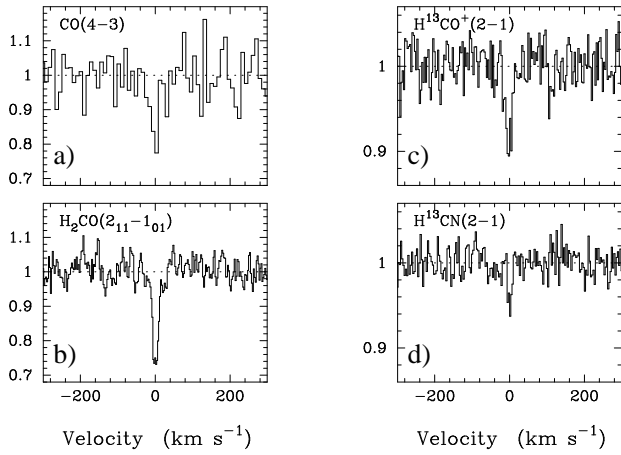


Fig. 5.— **a)** CO(4 $\leftarrow$ 3), **b)** H<sub>2</sub>CO(2<sub>11</sub>  $\leftarrow$ 1<sub>01</sub>), **c)** H<sup>13</sup>CO<sup>+</sup>(2 $\leftarrow$ 1) and **d)** H<sup>13</sup>CN(2 $\leftarrow$ 1) absorption at  $z=0.88582$ . All spectra except H<sub>2</sub>CO, have been obtained with the IRAM 30-m telescope. H<sub>2</sub>CO was observed with the 15-m SEST. The velocity resolution is 9.2 km s<sup>-1</sup> for the CO spectrum, 2.6 km s<sup>-1</sup> for the H<sub>2</sub>CO spectrum and 3.25 km s<sup>-1</sup> for the H<sup>13</sup>CO<sup>+</sup> and H<sup>13</sup>CN spectra. The total continuum level has been normalized to unity and the velocity scale is heliocentric in the restframe of the  $z=0.88582$  absorber.

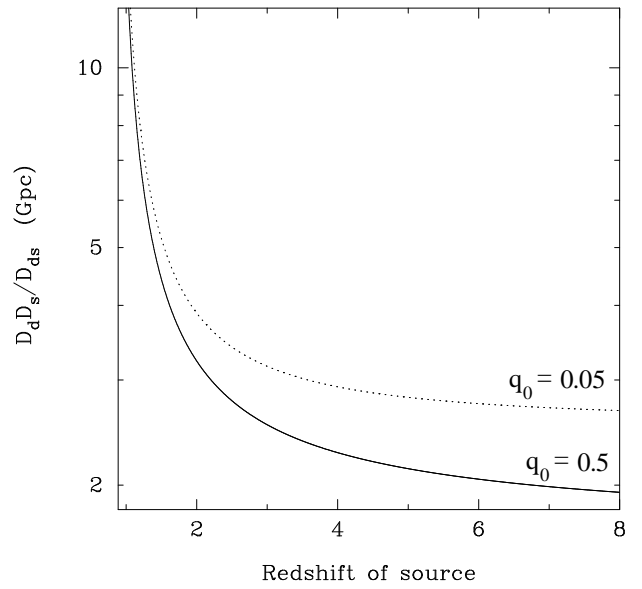


Fig. 6.— The distance parameter  $D = D_d D_s / D_{ds}$ , where  $D_d$  is the angular size distance between the observer and the deflector,  $D_s$  the distance between the observer and the source, and  $D_{ds}$  is the distance between the deflector and the source. In this plot the redshift of the deflector is held fixed at  $z=0.88582$ . The relation is given for a Hubble parameter  $H_0 = 75 \text{ km s}^{-1} \text{ Mpc}^{-1}$  and for  $q_0 = 0.5$  and  $q_0 = 0.05$ .

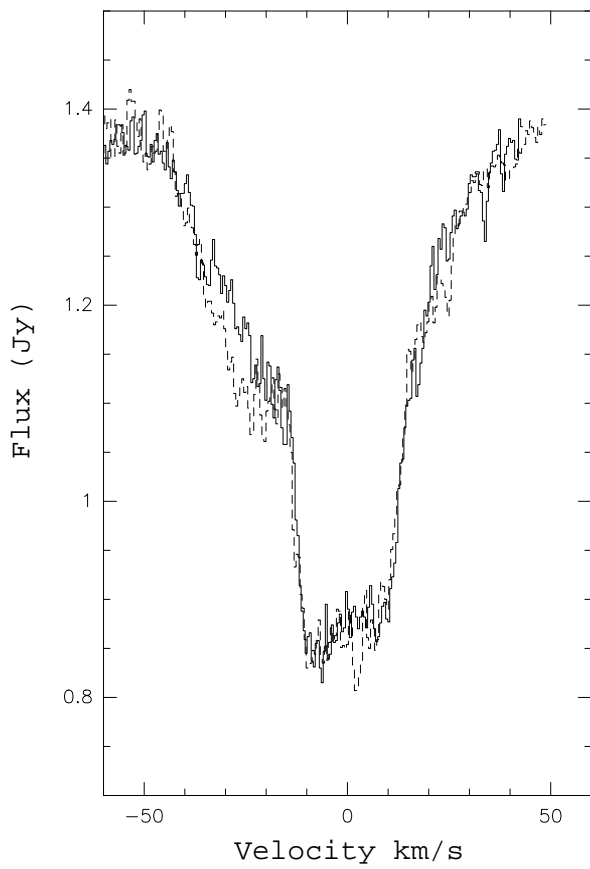


Fig. 7.— High spectral resolution ( $0.5 \text{ km s}^{-1}$ ) Plateau de Bure absorption profile in  $\text{HCO}+(2\leftarrow 1)$  in April 96 (full line) and September–October 1995 (dashed line).